

# Universal spatial inflation of human mobility

Lu Zhong<sup>1,2,6</sup>, Lei Dong<sup>3,6</sup>, Qi Wang<sup>4</sup>, Chaoming Song<sup>5</sup>, Jianxi Gao<sup>1,2\*</sup>

<sup>1</sup>*Department of Computer Science, Rensselaer Polytechnic Institute, Troy, NY, USA*

<sup>2</sup>*Network Science and Technology Center, Rensselaer Polytechnic Institute, Troy, NY, USA*

<sup>3</sup>*Institute of Remote Sensing and Geographical Information Systems, School of Earth and Space Sciences, Peking University, Beijing, China*

<sup>4</sup>*Department of Civil and Environmental Engineering, Northeastern University, Boston, MA, USA*

<sup>5</sup>*Department of Physics, University of Miami, Coral Gables, FL, USA*

<sup>6</sup>*These authors contributed equally: Lu Zhong, Lei Dong.*

*Email: gaoj8@rpi.edu*

**Understanding the interplay between egocentric preference and urban structure in shaping human mobility has profound implications for improving epidemic intervention, social equity, and urban resilience. However, numerous existing studies either solely identify the egocentric preferences—the anchoring effects from home or the impact of hierarchical urban structures. Here, we propose a network-based approach to present human mobility in both spatial and topological aspects within the urban system, using cell phone trajectory data from millions of users across three countries. By segmenting mobility trajectories into modules and examining their overlap with urban scales, we have observed the inflation law that the geospatial extent of these modules increases sub-linearly with their distance from home. Moreover, the egocentric preference for higher urban levels leads to this increase. This uni-**

**versal finding indicates that home-based preferences distort the hierarchical scales of human mobility in the urban environment, regardless of demographics or geography.**

Mobility is a critical aspect of human daily life<sup>1-3</sup>, with profound implications for addressing issues of disease transmission<sup>4</sup>, activity inequality<sup>5</sup>, and urban resilience<sup>6</sup>. The movement of humans closely resembles in many ways the Lévy flight of animals in the natural world<sup>7,8</sup>. The difference, however, is that human mobility is profoundly influenced by two social factors. The first is the egocentric preference<sup>9-11</sup> that many human activities are carried out with the home as an anchor, shaping their travels and interactions with their surroundings. The second factor is the hierarchical structure of the urban system that exhibits spatial scaling at multiple levels<sup>12,13</sup>, beginning with neighborhoods, escalating to cities, and ultimately encompassing states, provinces, and even countries. Recent research provides evidence that humans move across these hierarchical scales (the second factor)<sup>14,15</sup>, but how egocentric preference (the first factor) affects human mobility within the hierarchical urban system remains poorly understood. Here, we introduce a network-based approach<sup>16,17</sup> to effectively dictate individual preference in spatial distance and topological aspects, i.e., the route humans choose within urban systems in human trajectory<sup>11</sup>. We then segment individual trajectories into network modules and examine their alignment with the urban structure and relationship to home, revealing the interplay between home-based preference and urban structure in shaping mobility behavior.

Our analysis is based on high-resolution cell phone datasets from three countries with varying cultures and levels of development. The first dataset encompasses six months of global positioning

system trajectories from two million anonymous users in the United States (U.S.). The second and third datasets capture two weeks of call detail records from 300,000 anonymous users in Senegal and 50,000 anonymous users in Ivory Coast, respectively. We construct a network for each user’s trajectory by representing stay points as network nodes and the connections between consecutive stay points as edges. In the network, the weight of edges is determined by the reciprocal of the spatial distance between these stay points, meaning that smaller spatial distances yield larger edge weights (see Methods and Fig. S1-S2 for details).

To illustrate the impacts of egocentric preference, we use the Louvain method<sup>18,19</sup> to partition trajectory networks into multiple modules and examine the correlation between module characteristics and their distance from the user’s home. Figure 1a-b shows a user’s trajectory that has been partitioned into four modules based on spatial and topological proximity. Among the module characteristics (Figs. S3-S7), we measure the module spatial size  $r_c$  as the average distance of stay points to the module centroid and the module distance  $d_c$  as the distance from the module centroid to the home. As shown in Fig. 1b, the radius of the module increases when one moves farther away from home. Upon a thorough analysis of all trajectories in our datasets, we find that  $r_c$  and  $d_c$  follow a remarkably universal pattern,

$$r_c \sim d_c^\kappa, \tag{1}$$

where  $\kappa$  is approximately 0.6 for U.S. data across the West, Northeast, Midwest, and South regions (Fig. 1c,d,f,g). The exponent  $\kappa$  is approximately 0.56 for Senegal (Fig. 1e) and 0.55 for Ivory Coast (Fig. 1h). We refer to this pattern in human mobility as the “inflation law”, i.e., when humans move farther away from home, their exploration scope (module sizes) increases sub-linearly. To

verify the generality of this pattern, we perform two robustness checks. In the first experiment, we measure the module size using its convex hull. In the second experiment, we classified users based on their demographic attributes (e.g., age, gender, race, poverty level, household income, and home location). Results show that in addition to being robust across datasets in various regions (Fig. 1), the inflation law remains consistent across different measures of spatial module extent and diverse demographic populations (Extended Data Figs. 1-4).

To further understand the inflation law, we closely examine individual modules within the hierarchical interconnected urban system<sup>20</sup>. Using Boston, Massachusetts as an example (Fig. 2a), the hierarchical system is demonstrated by the interconnection of lower-level urban clusters through high-level urban clusters (see Methods). Generally, low-level clusters cover a small spatial range (e.g., neighborhoods) and provide simple urban functions, while high-level clusters cover a large spatial range (e.g., cities and regions) and provide complex functions. Figure 2b illustrates module networks of individuals at the destination Boston, Massachusetts. As shown in Fig. 2b-d, when individuals travel far from their homes, the module networks are across higher levels and span a larger geographical area. We evaluate the urban level of modules  $L_c$  as the minimum urban level encompassing over eighty percent of visited locations within the module. Specifically, when distances ( $d_c$ ) extend to 10km, 100km, and 1000km, the urban levels  $L_c$  of the modules exhibit a normal distribution centered around values of 1, 3, and 5, respectively. Concurrently, the module radius  $r_c$  expands to 4km, 15km, and 188km, corresponding to neighborhood, city, and state scales. These findings, when viewed from the perspective of the destination area, further validate the inflation law.

Upon analyzing all datasets, the urban level of modules when far from home can be illustrated by the relationship  $L_c \sim \log(d_c)$  in Fig. 2e. By examining the spatial radius  $R$  of urban levels and their relationship with distance  $d_c$ , we find the spatial radius of urban levels follows  $\log(R) \sim L_c \sim \log(d_c)$  and it aligns with the module radius  $r_c$  in generating the inflation law (Fig. 2f-g). These results indicate humans prioritize accessing resources, services, and facilities located at higher levels when distant from home. Given the truth that higher urban levels in larger spatial sizes, the preference for higher levels leads to the emergence of the inflation law.

In summary, we introduce the network-based segmentation of individual trajectories as a novel approach to comprehending human mobility patterns across geographical extents. By analyzing modules within individual trajectories with their distance from home, we reveal the egocentric preference and the urban hierarchical structure in jointly shaping human mobility. Urban structure enables mobility across different focal regions, culminating in the emergence of multiple modules in individual trajectories. Simultaneously, personal egocentric preferences of urban levels cause individuals to expand their exploration scopes within modules as they travel farther from home. This dual influence encapsulates the essence of the inflation law. This finding aligns with research thirty years ago that humans have distorted home-based preference of the hierarchical scales of the urban environment<sup>10</sup>. Furthermore, the inflation phenomenon resonates with the concept in Steinberg’s renowned illustration, “View of the World from 9th Avenue”<sup>21</sup>, which suggests that an individual’s perception of a region’s scales is influenced by its distance from their home. Future research, especially in cognitive science, will undoubtedly advance our understanding of the cognitive mechanisms underlying the inflation law. Lastly, using large-scale data from real-

world environments, this study provides new insights into understanding human mobility patterns within urban environments, which has significant implications for future research in improving urban living, transportation efficiency, and epidemic intervention.

## **Methods**

**Data.** Our analysis of human trajectories leverages three distinct datasets: one from the United States, another from Senegal, and a third from the Ivory Coast. We have rigorously classified the geographical positions of users within these datasets to a high degree of precision, utilizing the H3 geospatial indexing system<sup>22</sup> at a resolution of 12, corresponding to a cell with an edge length of approximately 9 meters. To ascertain the 'home' location of users, we identified the cell that each user visited most frequently during the night, specifically between the hours of 8 pm and 8 am.

The U.S. dataset is from anonymized location-based service records provided by Cuebiqu Inc. The raw dataset covers 42 million users from January to June 2020. Employing the Infostop algorithm<sup>23</sup>, we processed each user's trajectories to identify stay points, resulting in a selection of roughly 2.1 million users with records spanning over thirty days. When exploring demographic characteristics, our investigation is grounded in data derived from the American Community Survey (ACS). These datasets are stratified by census block groups. We, therefore, integrated trajectories linked to census block groups, offering insights into a spectrum of social, economic, and demographic across various regions in the U.S.

The Senegal dataset is based on anonymized call detail records supplied by the Data for

Development (D4D) Senegal Challenge<sup>3,24</sup>. It is from 2013, and the dataset is segmented into 25 discrete two-week intervals. Within each interval, roughly 44 million records are tied to mobile towers, attributed to approximately 300,000 randomly selected users.

The Ivory Coast dataset is based on anonymized call detail records supplied by the Data for Development (D4D) Ivory Coast Challenge<sup>3,24</sup>. It was collected between December 2011 and April 2012 and is split into two-week periods. It contains high-resolution trajectories of 50,000 randomly sampled individuals over the intervals.

**Extracting modules from human trajectory networks.** With our hypothesis that interconnected urban structures impact individual trajectories, we utilize networks to represent human trajectories. For each user’s trajectory  $T = \{\theta_1, \dots, \theta_i, \dots\}$  where  $i$  are the sequence index of stay points, we build the trajectory network  $G(T)$  where each stay point as the node and consecutive travels between two stay points as the edges. To characterize  $G(T)$  in geographical space, we define the edge weight set  $W(T) = \{w(\theta_1, \theta_2), \dots, w(\theta_i, \theta_{i+1}), \dots\}$  and  $w(\theta_i, \theta_{i+1})$  is denoted as

$$w(\theta_i, \theta_{i+1}) = \log\left(\frac{\hat{d}}{d(\theta_i, \theta_{i+1})}\right) \quad (2)$$

where  $d(\theta_i, \theta_{i+1})$  is the spatial distance between stay points  $\theta_i$  and  $\theta_{i+1}$ . The parameter  $\hat{d}$  corresponds to the max jump distance, constrained by the geographical size of a country. For example,  $\hat{d}$  equals 4,000km for the U.S., and  $\hat{d}$  equals 1,000km for Senegal and Ivory Coast. It is worth noting that  $\hat{d} \geq d(\theta_i, \theta_{i+1})$  ensures the weights are all non-negative. The log transformation is designed to amplify the influence of shorter distances by assigning them greater weight, an approach known as inverse distance weighting (IDW). This technique is underpinned by the fundamental principle

known as Tobler’s first law of geography<sup>25</sup>, which states that entities in close proximity have a greater likelihood of interaction and connection than those farther apart.

Next, we use the community detection method<sup>26</sup> to detect modules in the weighted directed trajectory network  $G(T)$ . We employ a stringent criterion to ensure that modules, denoted as  $g$ , are coherent regarding spatial proximity and not arbitrarily inclusive of unrelated stay points. We also exclude staying points that are less than half the distance between the module’s centroid and the home location. Additionally, modules with fewer than three locations are removed.

The characterization of these detected modules is multi-faceted. Firstly, we represent each module using its centroid, a pivotal point that encapsulates its spatial center. Additionally, we measure the distance from this centroid to the corresponding home location. Moreover, we quantify the module’s spatial extent by calculating the convex hull area and the module radii, which signifies the average distance from all stay points within the module to its centroid. Furthermore, we analyze the number of modules of each user and their visitation frequencies (Figs. S3-S7).

**Delineating hierarchical levels in urban space.** To ensure that the hierarchical levels represent the spatial scales in urban space, we employ the Hexagonal Hierarchical Spatial Index. This indexing system divides urban space into discrete cells, each location being assigned a cell identifier, and higher resolutions are composed of lower resolutions. Specifically, we use divisive hierarchical clustering techniques and recursively split clusters at resolution from 7 to 1, with hexagon edge lengths varying from 1 kilometer to 418 kilometer. We first consider all location indexes at resolution  $\sigma = 1$  in the dataset as a single cluster. We recursively split the cluster into multiple

sub-clusters using the Louvain method on flow network between location index at higher resolution  $\sigma + 1$ . This iterative process continues until resolution  $\sigma = 7$  is reached. As a result, we obtain sub-clusters at varying resolutions and set them from high to low levels  $L$  in the hierarchy.

To compare the modules within each trajectory with urban levels, we assign the module (subnetwork  $g_i$ ) assigned level  $L_c = L$  if  $L$  is the minimal level that satisfied  $\frac{N_i \cap N_L}{N_L} \geq 0.8$ , where  $N_L$  is the set of locations within level  $L$  and  $N_i$  is the set of location within module  $g_i$ . This criterion ensures that a significant portion of locations within the module is covered by level  $L$ .

## References

1. Gonzalez, M. C., Hidalgo, C. A. & Barabasi, A.-L. Understanding individual human mobility patterns. *Nature* **453**, 779–782 (2008).
2. Simini, F., González, M. C., Maritan, A. & Barabási, A.-L. A universal model for mobility and migration patterns. *Nature* **484**, 96–100 (2012).
3. Schläpfer, M. *et al.* The universal visitation law of human mobility. *Nature* **593**, 522–527 (2021).
4. Belik, V., Geisel, T. & Brockmann, D. Natural human mobility patterns and spatial spread of infectious diseases. *Physical Review X* **1**, 011001 (2011).
5. Althoff, T. *et al.* Large-scale physical activity data reveal worldwide activity inequality. *Nature* **547**, 336–339 (2017).
6. Barbosa, H. *et al.* Human mobility: Models and applications. *Physics Reports* **734**, 1–74 (2018).
7. Brockmann, D., Hufnagel, L. & Geisel, T. The scaling laws of human travel. *Nature* **439**, 462–465 (2006).
8. Rhee, I. *et al.* On the Levy-walk nature of human mobility. *IEEE/ACM Transactions on Networking* **19**, 630–643 (2011).
9. Pappalardo, L., Manley, E., Sekara, V. & Alessandretti, L. Future directions in human mobility science. *Nature Computational Science* **3**, 588–600 (2023).

10. Lloyd, R. & Heivly, C. Systematic distortions in urban cognitive maps. *Annals of the Association of American Geographers* **77**, 191–207 (1987).
11. Hirtle, S. C. & Jonides, J. Evidence of hierarchies in cognitive maps. *Memory & Cognition* **13**, 208–217 (1985).
12. Batty, M. Hierarchy in cities and city systems. *Hierarchy in Natural and Social Sciences* 143–168 (2006).
13. Xu, Y. *et al.* Urban dynamics through the lens of human mobility. *Nature Computational Science* **3**, 611–620 (2023).
14. Bassolas, A. *et al.* Hierarchical organization of urban mobility and its connection with city livability. *Nature Communications* **10**, 4817 (2019).
15. Alessandretti, L., Aslak, U. & Lehmann, S. The scales of human mobility. *Nature* **587**, 402–407 (2020).
16. Barthélemy, M. Spatial networks. *Physics Reports* **499**, 1–101 (2011).
17. Bagrow, J. P. & Lin, Y.-R. Mesoscopic structure and social aspects of human mobility. *PloS ONE* **7**, e37676 (2012).
18. Newman, M. E. Modularity and community structure in networks. *Proceedings of the National Academy of Sciences* **103**, 8577–8582 (2006).
19. Schneider, C. M., Belik, V., Couronné, T., Smoreda, Z. & González, M. C. Unravelling daily human mobility motifs. *Journal of The Royal Society Interface* **10**, 20130246 (2013).

20. Roth, C., Kang, S. M., Batty, M. & Barthélemy, M. Structure of urban movements: polycentric activity and entangled hierarchical flows. *PloS ONE* **6**, e15923 (2011).
21. Steinberg, S. View of the world from 9th avenue. *The New Yorker* (1976).
22. H3: Uber's hexagonal hierarchical spatial index. <https://www.uber.com/blog/h3/>. Accessed: 2023-09-01.
23. Aslak, U. & Alessandretti, L. Infostop: Scalable stop-location detection in multi-user mobility data. *arXiv preprint arXiv:2003.14370* (2020).
24. De Montjoye, Y.-A., Smoreda, Z., Trinquart, R., Ziemlicki, C. & Blondel, V. D. D4D-Senegal: The second mobile phone data for development challenge. *arXiv preprint arXiv:1407.4885* (2014).
25. Miller, H. J. Tobler's first law and spatial analysis. *Annals of the Association of American Geographers* **94**, 284–289 (2004).
26. Fortunato, S. Community detection in graphs. *Physics Reports* **486**, 75–174 (2010).

**Acknowledgments** We thank Jinzhu Yu for his assistance with pre-processing the mobility data and fruitful discussion. J.G. and L.Z. acknowledge the support of the US National Science Foundation under Grant No. 2047488. L.D. was supported by the Fundamental Research Funds for the Central Universities, Peking University. Q.W. acknowledges the support of the US National Science Foundation under Grant No. 2125326.

**Author contributions** L.Z., L.D., Q.W., and J.G. conceived the project and designed the experiments; L.Z. and Q.W. collected and analyzed the data; L.Z., L.D., J.G., and C.S. carried out theoretical calculations and performed the experiments; all authors wrote and edited the manuscript.

**Competing interests** The authors declare no competing interests.

**Correspondence and requests for materials** should be addressed to J.G.

**Additional information** Supplementary Notes 1-2, including Supplementary Figures 1-6, Supplementary Tables 1.

**Data and code availability** Data files and the Python script have been deposited in [https://github.com/lucinezhong/Spatial\\_inflation](https://github.com/lucinezhong/Spatial_inflation)

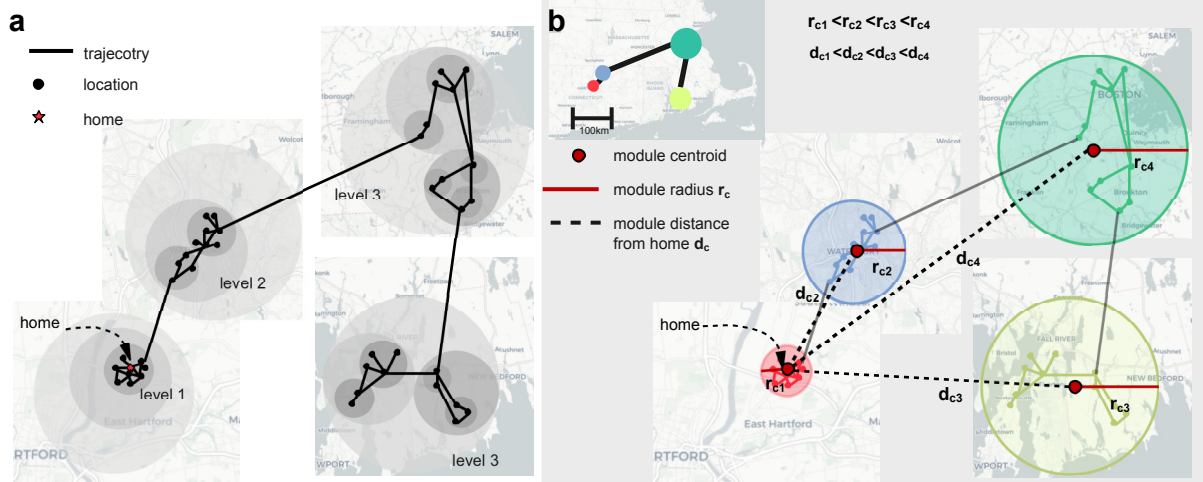


Figure 1: **The spatial inflation of modules.** (a) Trajectory of anonymized cell phone users in the urban environment of hierarchical levels. The star marks the users' home location. By representing trajectories as networks and applying the Louvain method, (b) the example trajectory network is divided into four modules, each encompassing spatially and topologically proximate locations. Modules located far from home are in larger spatial coverage. By analyzing all U.S., Senegal, and Ivory Coast data, (c-h) module radius  $r_c$  increases with distance from home  $d_c$  in a power-law manner,  $r_c \sim d_c^\kappa$ . Specifically, for U.S. data in the West, Northeast, Midwest, and South regions, the value of  $\kappa$  is approximately 0.60. For Senegal and Ivory Coast data,  $\kappa$  is approximately 0.56 and 0.55, respectively.

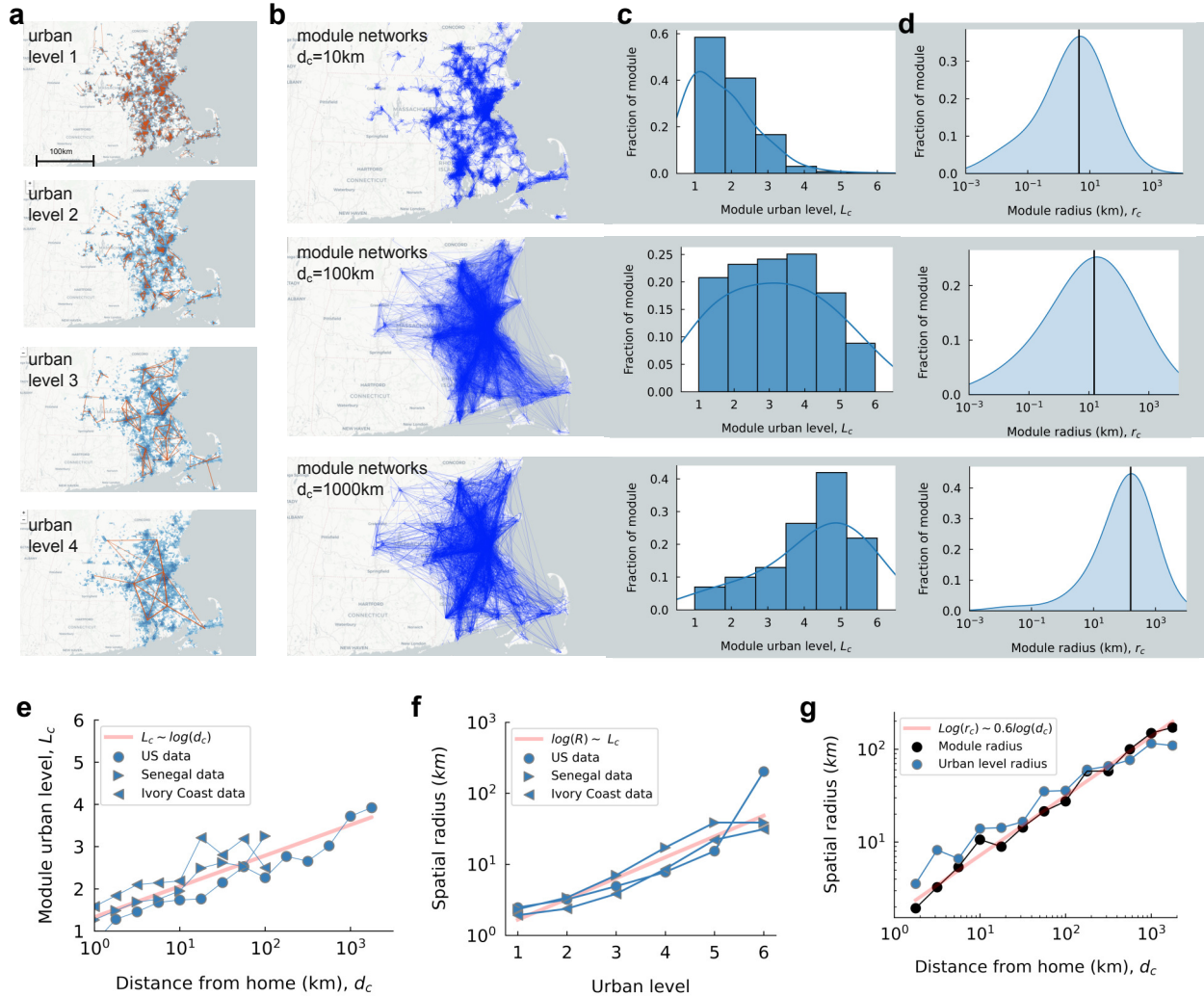
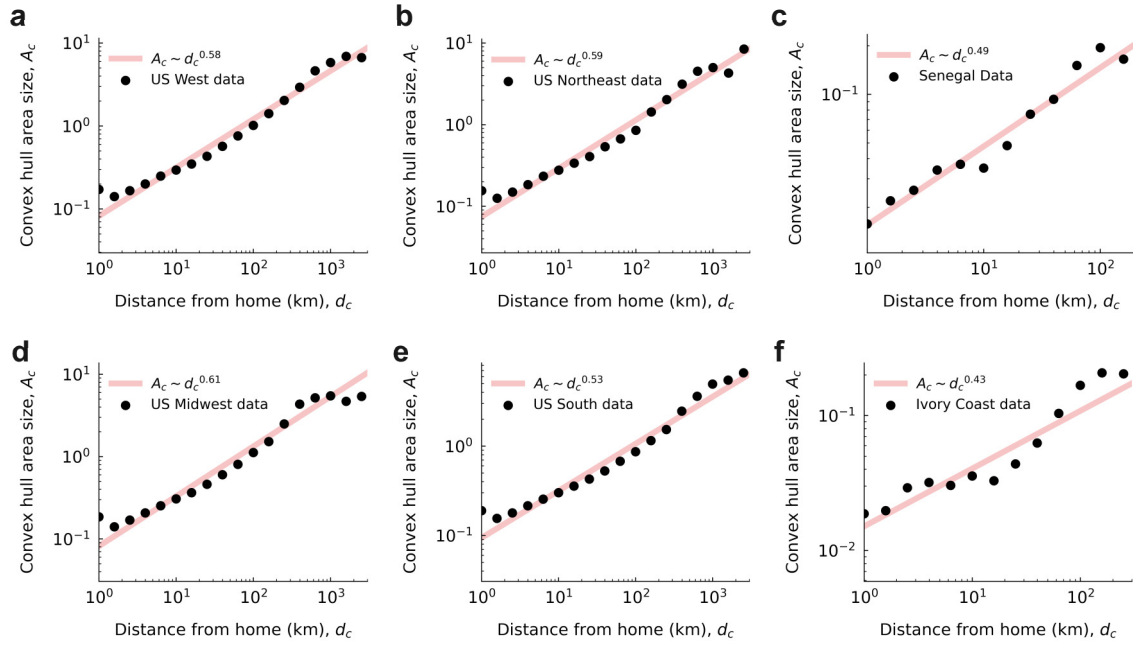
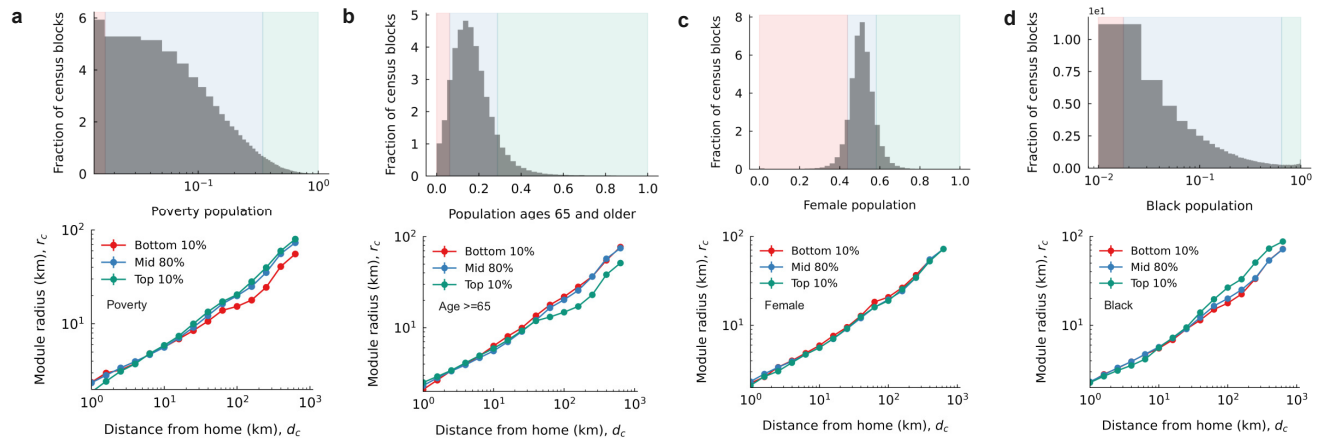


Figure 2: **Egocentric preference of hierarchical levels leads to inflation law.** With Boston, Massachusetts as the example, **(a)** the urban environment is structured into four hierarchical levels, with lower levels being connected by higher ones. **(b)** Users' module networks at varying distances from home, denoted as  $d_c$  with values of  $10\text{km}$ ,  $100\text{km}$ , and  $1000\text{km}$ . Modules are assigned to a specific level  $L_c$  if the module is covered by that level at an 80% threshold. **(c)** The distribution of urban levels for modules  $L_c$ . As the distance from home increases, humans show a higher preference for moving at higher levels. The home-based preferences result in a corresponding larger module radius in the distribution of modules' radius  $r_c$  **(d)**. **(e)** Urban levels for modules at varying distances from home,  $L_c \sim \log(d_c)$ . **(f)** Spatial size of urban levels for U.S., Senegal, and Ivory Coast data,  $\log(R) \sim L_c \sim \log(d_c)$ . **(g)** The overlap between the spatial radius of urban levels and the module radius at varying distances from home.

## Extended Data Figures

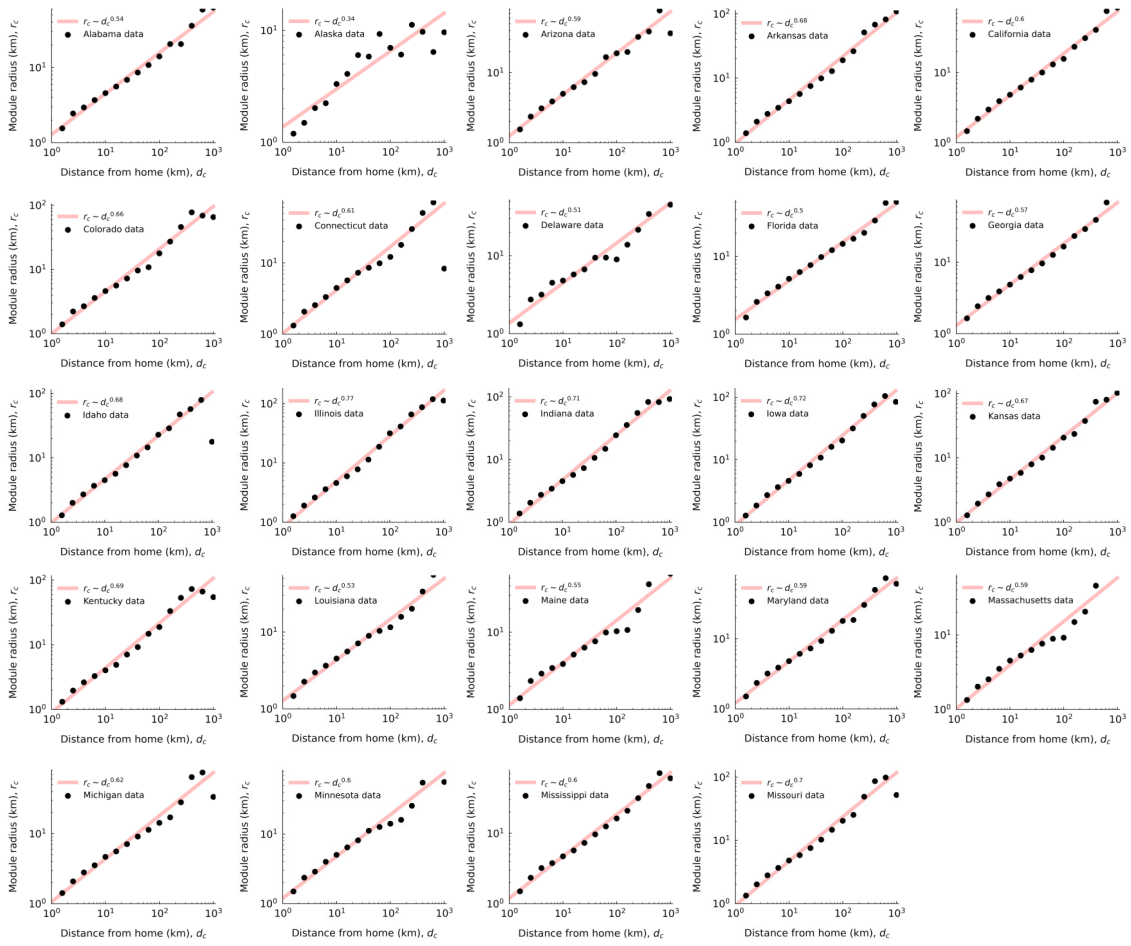


**Extended Data Fig. 1: The spatial inflation of modules regarding convex hull area size.** Module convex hull area size,  $A_c$ , increases sub-linearly with its distance from home  $d_c$ . The exponent is around 0.55 for the U.S. data, 0.52 for the Senegal data, and 0.44 for the Ivory Coast data.

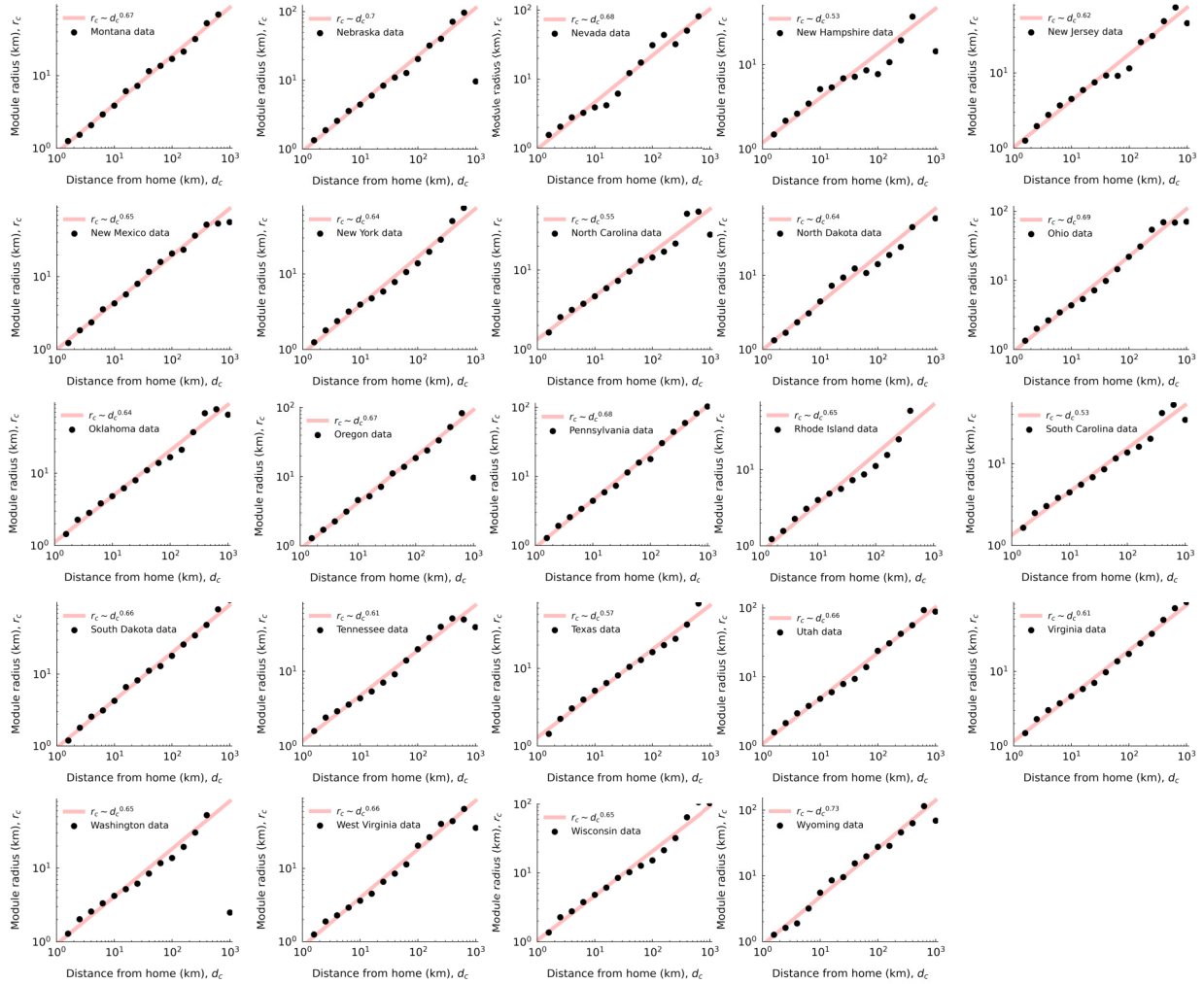


**Extended Data Fig. 2: The spatial inflation of modules across populations in different demographic attributes.**

By categorizing users based on the proportions of the poverty population in their home locations (a), the elderly population (age 65 and older) (b), the female population (c), and the black population (d), the spatial inflation of module remains consistent across various user groups.



**Extended Data Fig. 3: Part-1-The spatial inflation of modules for populations in different states.** By categorizing users based on the states of their home locations, the spatial inflation of the module remains consistent.



**Extended Data Fig. 4: Part-2-The spatial inflation of modules for populations in different states.** By categorizing users based on the states of their home locations, the spatial inflation of the module remains consistent.

## Contents

|          |   |           |
|----------|---|-----------|
| <b>1</b> | <b>Supplementary Note 1: Trajectory network modules</b>         | <b>21</b> |
| 1.1      | Datasets . . . . .  | 21        |
| 1.3      | Network modules: topological and spatial properties . . . . .   | 21        |
| <b>2</b> | <b>Supplementary Note 2: Spatial inflation robustness check</b> | <b>22</b> |
| 2.1      | Populations in different demographic attributes . . . . .       | 22        |
| 2.2      | Populations in different regions . . . . .                      | 23        |
| 2.3      | COVID-19 lockdown effects . . . . .                             | 23        |

## 1 Supplementary Note 1: Trajectory network modules

**1.1 Datasets** We use the fundamental measures of jump distance and waiting time to characterize human mobility in the three datasets, see in Table. 1. As shown in Fig. 5 and Fig. 6, the jump-distance distributions are approximated by  $P(\Delta r) \sim \Delta r^{-(1+\alpha)}$  where  $\alpha = 0.77, 1.22, 1.23$  respectively for United States, Senegal, and Ivory Coast data. The waiting-time distributions are approximated  $P(\Delta t) \sim \Delta t^{-(1+\beta)}$  where  $\beta = 0.61, 0.27, 0.88$  respectively. When we closely examine travels that originate at distances from home ( $d$ ) of 10 km, 100 km, and 1000 km while excluding journeys back home, we observe a trend in Fig. 5d-f. As  $d$  increases, the distribution of jump lengths tends to have smaller exponents. Taking the United States data as an example, we find  $\alpha$  values of 0.89, 0.59, and 0.20 for  $d = 10, 100, 1000$  km, respectively. This same pattern is observed in the data from Senegal and Ivory Coast. This trend implies that when individuals travel far from home, they are more likely to initiate long-distance travel. It means that the power-law distribution of jump distances is not uniform for all users at any distance from home. However, when examining the waiting-time distribution in Fig. 6d-f, we observe that this distribution remains consistent regardless of the distance  $d$ . The observations prompt us to explore the fair approach to segment human travel trajectories and to find the underlying fundamental mechanism driving the varying jump distance at  $d$ .

**1.2 Network modules: topological and spatial properties** Given our assumption that individual trajectories are impacted by interconnected urban structures, we utilize a network representation to depict human trajectories, with nodes representing locations and edge weights symbolizing spatial distances, as described in the Methods section. We then extract modules from these human trajectory networks. Fig. 7 displays the distribution of the number of extracted modules, revealing that human networks exhibit segmentability with an average presence of multiple modules. Following segmentation, we proceed to analyze the topological and spatial properties of these modules.

**Module topological size.** We use the number of nodes and edges with network modules to characterize the topological size. As shown in Fig. 8 and Fig. 9, we use the home as the reference point to identify module location  $d_c$ . As the module distance from home,  $d_c$  increases, both the number of nodes (representing unique locations within modules) and the number of edges (representing travels within modules) decrease. In terms of network topology, module sizes tend to become smaller when far from home.

**Module spatial size.** For module spatial size, we use the radius  $r_c$ , that is, the average distance from locations to the molecule centroid to measure the module size. We find that module radius sub-linearly increases with module distance to home in logarithmic scales,  $r_c \sim d_c^k$ . To guarantee the finding is objective and systematic, we also use the area size ( $A_c$ ) of the convex hull formed by visited locations within modules to characterize module size. Extended Data Fig. 1 shows that in the United States, Senegal, and Ivory Coast data, the modules' convex hull size ( $A_c$ ) correlates with  $d_c$  in logarithmic scales,  $A_c \sim d_c^{k'}$ . It again justifies that as humans venture farther away from their homes, the size of modules increases exponentially with home serving as the reference point.

**Module visitation.** Besides module size, we depict the visitation frequency of modules in Fig. 10. The visitation frequency decays with module distance  $d_c$ , indicating that humans are less likely to visit modules far from home.

## 2 Supplementary Note 2: Spatial inflation robustness check

**2.1 Populations in different demographic attributes** We also categorize the users' trajectories according to their home locations' demographic attributes (e.g., age, gender, race and ethnicity, and poverty level) to inspect the module size for each group of individuals in Extended Data Fig. 2.

Individuals with different demographic features show no significant difference for a relationship,  $r_c \sim d_c^\kappa$ . It means the spatial inflation is consistent across user groups living in regions with different demographic attributes.

**2.2 Populations in different regions** To ensure the universality of spatial inflation across different subpopulations, we categorize users' trajectories based on which states their home locations belong to in the United States data, as shown in Extended Data Fig. 3-4. We exclude states with fewer than 1000 trajectories. Interestingly, individuals from different states exhibit consistent inflation patterns. While the exponent  $\kappa$  varies from state to state, it consistently keeps around a value of approximately 0.59.

**2.3 COVID-19 lockdown effects** The COVID-19 lockdown is known to have altered people's mobility patterns, with the most notable changes observed in U.S. datasets being a decrease in the frequency of travel. However, despite these changes, we consistently find that the spatial inflation phenomenon, where the module radii increase with the module distance ( $r_c \sim d_c^\kappa$ ), remains unchanged for both the pre-lockdown and post-lockdown periods, as illustrated in Fig. 11.

1. Gonzalez, M. C., Hidalgo, C. A. & Barabasi, A.-L. Understanding individual human mobility patterns. *Nature* **453**, 779–782 (2008).
2. Simini, F., González, M. C., Maritan, A. & Barabási, A.-L. A universal model for mobility and migration patterns. *Nature* **484**, 96–100 (2012).
3. Schläpfer, M. *et al.* The universal visitation law of human mobility. *Nature* **593**, 522–527 (2021).
4. Belik, V., Geisel, T. & Brockmann, D. Natural human mobility patterns and spatial spread of infectious diseases. *Physical Review X* **1**, 011001 (2011).

5. Althoff, T. *et al.* Large-scale physical activity data reveal worldwide activity inequality. *Nature* **547**, 336–339 (2017).
6. Barbosa, H. *et al.* Human mobility: Models and applications. *Physics Reports* **734**, 1–74 (2018).
7. Brockmann, D., Hufnagel, L. & Geisel, T. The scaling laws of human travel. *Nature* **439**, 462–465 (2006).
8. Rhee, I. *et al.* On the Levy-walk nature of human mobility. *IEEE/ACM Transactions on Networking* **19**, 630–643 (2011).
9. Pappalardo, L., Manley, E., Sekara, V. & Alessandretti, L. Future directions in human mobility science. *Nature Computational Science* **3**, 588–600 (2023).
10. Lloyd, R. & Heivly, C. Systematic distortions in urban cognitive maps. *Annals of the Association of American Geographers* **77**, 191–207 (1987).
11. Hirtle, S. C. & Jonides, J. Evidence of hierarchies in cognitive maps. *Memory & Cognition* **13**, 208–217 (1985).
12. Batty, M. Hierarchy in cities and city systems. *Hierarchy in Natural and Social Sciences* 143–168 (2006).
13. Xu, Y. *et al.* Urban dynamics through the lens of human mobility. *Nature Computational Science* **3**, 611–620 (2023).
14. Bassolas, A. *et al.* Hierarchical organization of urban mobility and its connection with city livability. *Nature Communications* **10**, 4817 (2019).
15. Alessandretti, L., Aslak, U. & Lehmann, S. The scales of human mobility. *Nature* **587**, 402–407 (2020).

16. Barthélemy, M. Spatial networks. *Physics Reports* **499**, 1–101 (2011).
17. Bagrow, J. P. & Lin, Y.-R. Mesoscopic structure and social aspects of human mobility. *PloS ONE* **7**, e37676 (2012).
18. Newman, M. E. Modularity and community structure in networks. *Proceedings of the National Academy of Sciences* **103**, 8577–8582 (2006).
19. Schneider, C. M., Belik, V., Couronné, T., Smoreda, Z. & González, M. C. Unravelling daily human mobility motifs. *Journal of The Royal Society Interface* **10**, 20130246 (2013).
20. Roth, C., Kang, S. M., Batty, M. & Barthélemy, M. Structure of urban movements: polycentric activity and entangled hierarchical flows. *PloS ONE* **6**, e15923 (2011).
21. Steinberg, S. View of the world from 9th avenue. *The New Yorker* (1976).
22. H3: Uber’s hexagonal hierarchical spatial index. <https://www.uber.com/blog/h3/>. Accessed: 2023-09-01.
23. Aslak, U. & Alessandretti, L. Infostop: Scalable stop-location detection in multi-user mobility data. *arXiv preprint arXiv:2003.14370* (2020).
24. De Montjoye, Y.-A., Smoreda, Z., Trinquart, R., Ziemlicki, C. & Blondel, V. D. D4D-Senegal: The second mobile phone data for development challenge. *arXiv preprint arXiv:1407.4885* (2014).
25. Miller, H. J. Tobler’s first law and spatial analysis. *Annals of the Association of American Geographers* **94**, 284–289 (2004).
26. Fortunato, S. Community detection in graphs. *Physics Reports* **486**, 75–174 (2010).

Table 1: Statistics of trajectory data. Here "m" stands for one million.

|                | Time period        | Total users (m) | Total records (m) | Records |        | Days |        |
|----------------|--------------------|-----------------|-------------------|---------|--------|------|--------|
|                |                    |                 |                   | mean    | median | mean | median |
| US             | 2020-01 to 2020-06 | 43              | 481,282           | 11,308  | 2,268  | 68   | 7      |
| US (processed) | 2020-01 to 2020-06 | 2.1             | 599               | 284     | 254    | 45   | 40     |
| Senegal        | 2013-01 to 2013-12 | 0.32            | 44                | 138     | 86     | 12   | 13     |
| Ivory coast    | 2011-12 to 2012-04 | 0.05            | 0.508             | 101     | 48     | 9    | 11     |

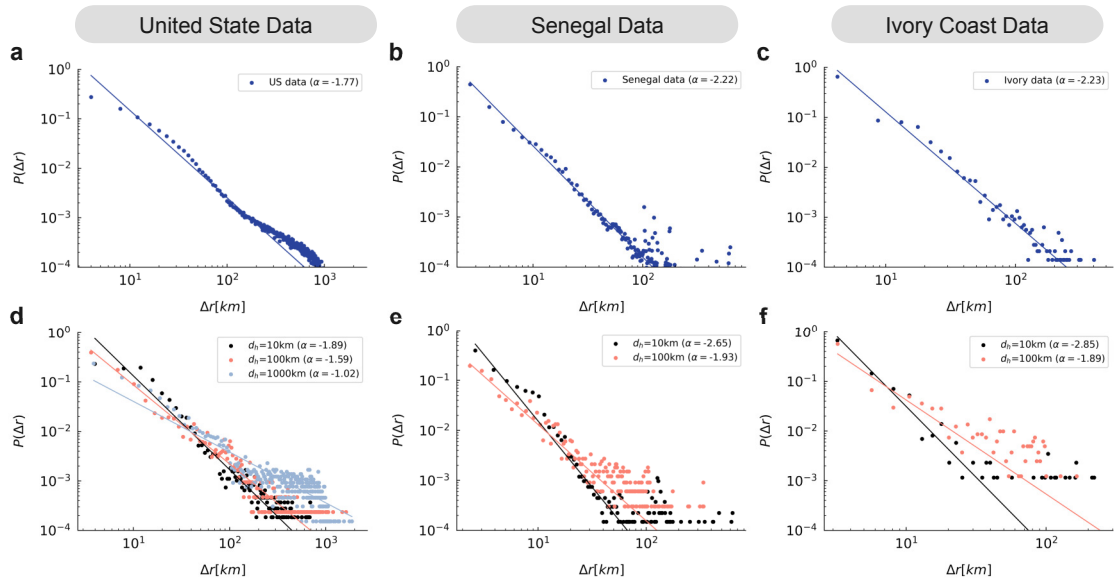


Figure 5: **Jump distance distribution for the United States, Senegal, and Ivory Coast data.** (a,b,c) Jump distance  $\Delta r$ , follows a power-law distribution characterized by  $P(\Delta r) \sim \Delta r^{-(1+\alpha)}$ . (d,e,f) Jump distance distribution if travel initiate at  $d_h = 10, 100, 1000$  km, respectively, with the exponent  $\alpha$  becoming smaller.

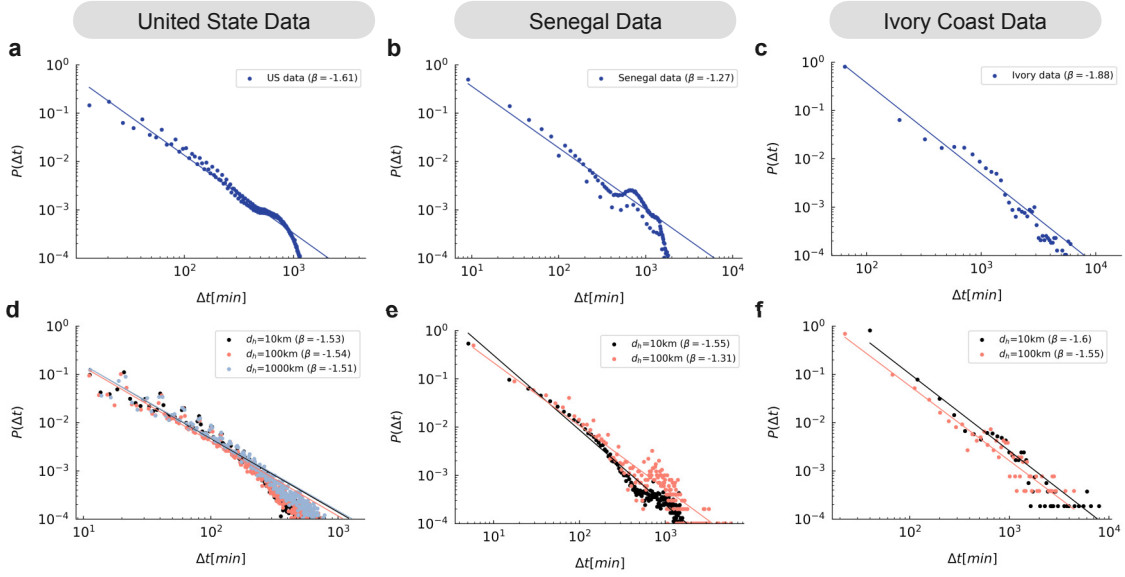


Figure 6: **Stay time distribution for the United States, Senegal, and Ivory Coast data.** (a,b,c) Stay time  $\Delta t$ , follows a power-law distribution characterized by  $P(\Delta t) \sim \Delta t^{-(1+\beta)}$ . (d,e,f) Stay time distribution if travel initiate at  $d_h = 10, 100, 1000$  km, respectively. The exponent  $\beta$  keeps no substantial change.

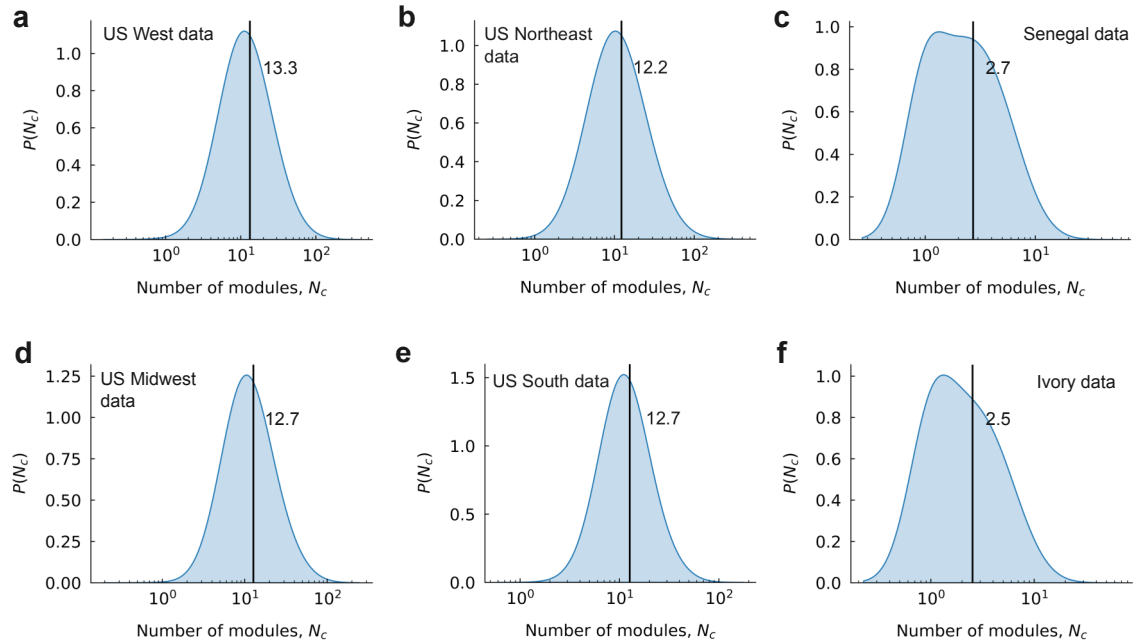


Figure 7: **Module counts within user trajectory networks for data from the United States, Senegal, and Ivory Coast data.** Users in the United States dataset typically have an average of twelve modules. As for the Senegal and Ivory Coast data, which are Detail Records with lower resolution, users typically have an average of three modules. Human trajectory networks exhibit segmentability.

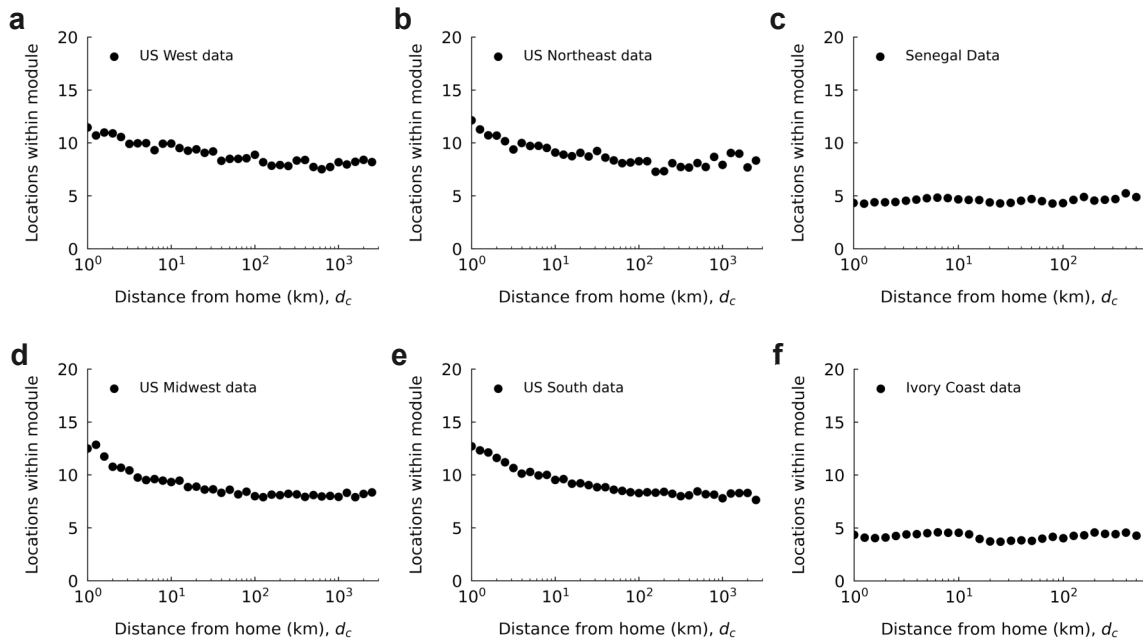


Figure 8: **Locations (Nodes) within modules for data from the United States, Senegal, and Ivory Coast data.** As the module distance increases, the counts of locations within modules slightly decrease. locations count decreases.

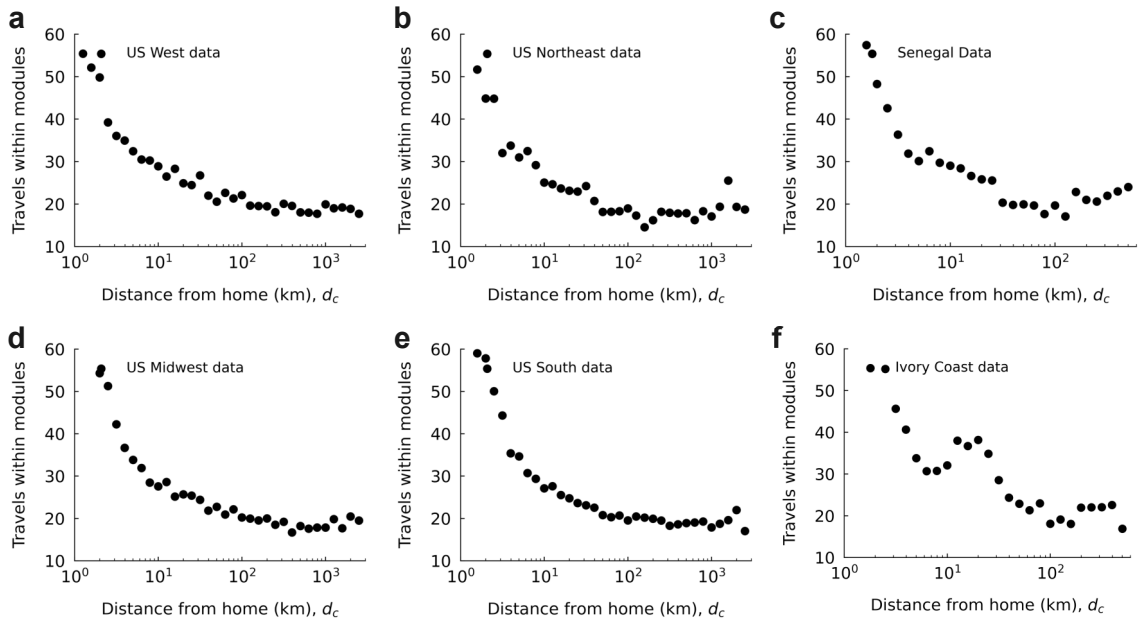


Figure 9: **Travels (Edges) within modules for data from the United States, Senegal, and Ivory Coast data.** As the module distance increases, the counts of travels within modules decrease.

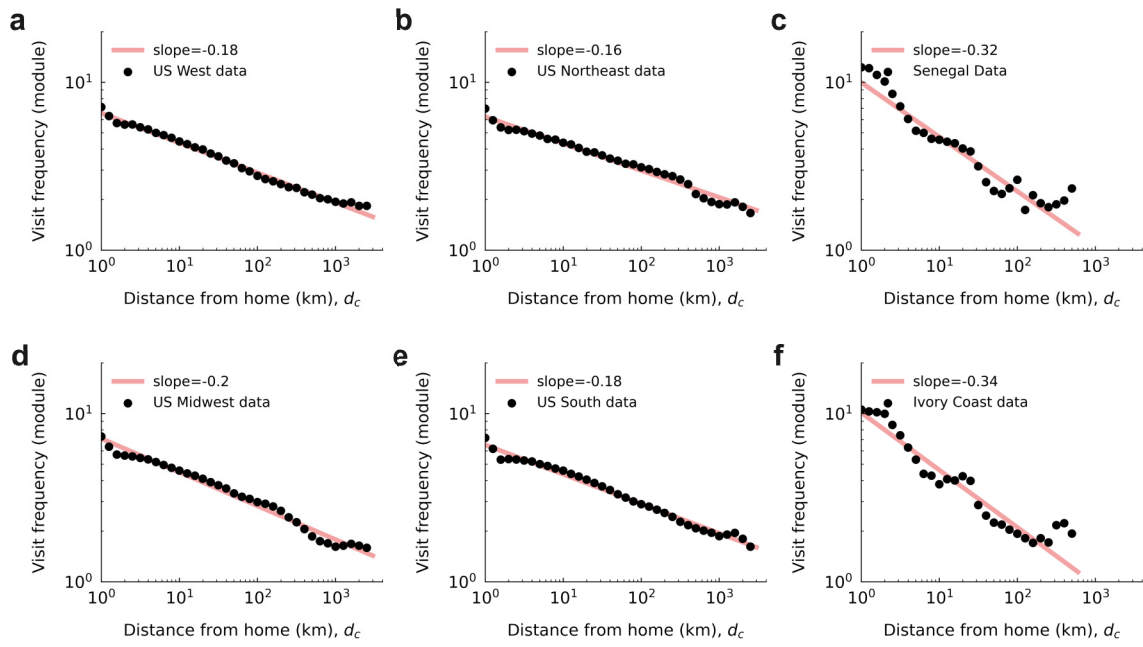


Figure 10: **Visitation frequency of module for data from the United States, Senegal, and Ivory Coast data.** As the module distance increases, the visitation frequency decreases.

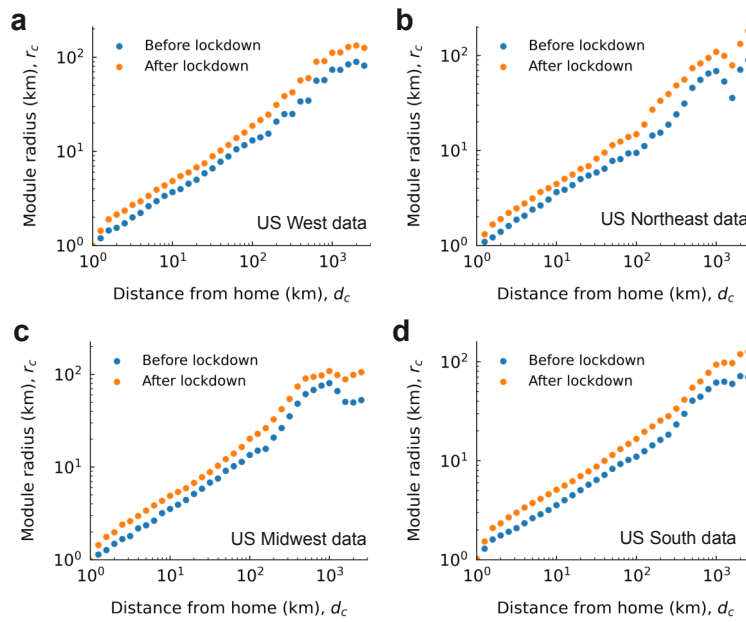


Figure 11: **The spatial inflation of modules before-lockdown period and after-lockdown period.** We set March 11 as the date to split the U.S. data into the before-lockdown period and after-lockdown period.